Designing Modular Reflective EM Skins to Improve Wireless Coverage in Urban Areas

P. Rocca, P. Da Rù, N. Anselmi, M. Salucci, G. Oliveri, and A. Massa

2024/06/28

Contents

1 Summary

1.1 Activity goal

The activity presented in this document aims at improving the performance of an urban communication scenario through the intelligent use of a "*smart skin*" embedded in the facade of a building. In the scope of telecommunications, the term smart skin refers to a device that offers a set of functionalities related to the manipulation of the EM waves in the system, and that is most interestingly used to redirect an impinging EM wave towards a desired direction, which creates the possibility for it to be properly engineered in order to improve the communication characteristics of the surrounding environment, such as the average per-user capacity or the overall spatial coverage. In the present document, the employment of a smart skin has been considered to improve the coverage satisfaction of a hypothetical area where the signal of the nearest Base Station (**BS**) arrives with a strong attenuation, due to natural or artificial obstacles in the path - generally referred to as a "*blind spot*". Furthermore, the deployment complexity and the visual impact that similar devices would have are considered, as it could not only increase installation and maintenance costs, but it could also become an issue for specific deployments in historic city centers or similarly regulated urban areas. Considering this, the final problem is formulated as a multi-objective optimization problem, where the goal is achieving the best coverage satisfaction while maintaining the lowest number of active surfaces on the smart skin.

1.2 Activity overview

1.2.1 Literature analysis

The first step of the activity has been an analysis of the most recent and most important productions of the literature in the field of metasurfaces, with a thorough review of the papers that showed promising characteristics for the desired final goal of the activity. Once the best candidate had been chosen, a deep mathematical formulation of the problem was produced, to isolate the formulas that were useful for the application of interest - i.e., those referred to the contribution of the smart skins to the final electric field - and to prepare the ground for their software implementation.

1.2.2 Software implementation

The software implementation has been performed, in line with the standard of the research center, utilizing Fortran as programming language for the core source code, bash scripts for the runners used to handle input and outputs of the core program, and Gnuplot scripts for the generation of the various representations of the final results. After the implementation was finished, it has been validated against the results obtained in the original reference, to verify the correct functioning of the software on which the rest of the activity would be based. The validation was accompanied by a study on the effects that the different parameters of the system had on the final result, in order to further corroborate, with graphical feedback, the behavior expected from the mathematical formulas.

Once the software that models the operation of a single metasurface was proven valid, it was further developed in order to include the consideration of multiple surfaces and multiple observation points. This addition allows for a better modelling of a real communication scenario, as the final deployment would be composed of a matrix of metasurfaces to create the

smart skin itself, and a set of observers scattered in the blind area to evaluate the actual effect of the proposed solution in multiple points.

1.2.3 Urban scenario simulation and optimization

Once the base software was proven valid, it was paired with the research center's proprietary optimizer ESPRESSO in order to be used in the definition of a multi-objective optimization problem. As previously mentioned, the final problem consists in the optimization of two conflicting cost functions:

1. the coverage satisfaction of the communication system, i.e., an assessment of how much the electric field received by users scattered inside the blind spot region differs from an a-priori fixed threshold;
2. the complexity of the smart skin deployment, i.e., the percentage of metasurfaces present on the building facade with respect to the maximum positions available.

The goal of the activity therefore is not the production of a perfect solution for the problem, but rather the definition of a series of "best compromises" between two conflicting properties that define the system.

These simulations have been performed at first in a simple scenario, in order to evaluate and better understand the smart skin behaviour when its dimensions and complexity are increased, and subsequently on a more realistic one, where the position of the single metasurfaces could not be arbitrarily chosen to be a convenient grid-like structure, but would need to be evaluated during the design of the system on the basis of the available space on the real facade of the building on which it would be applied.

2 Introduction

2.1 Document Organization

The present document is divided into two parts:

1. The first part is dedicated to a review of the State of the Art (*SoA*), starting from a large-scope recollection of the most significant contribution in the literature and moving towards more and more thorough analysis, comparing some of the considered contributions, highlighting the most interesting characteristics, and subsequently studying and reviewing three of them in specific detail,
2. The second part presents the code implementation of the problem, the definition of the working scenario, the obtained results, and all the data and formulations regarding the "practical" part of the activity, starting from the benchmark validation of the reference paper and ending with a multi-objective optimization of a urban scenario in which an EM smart skin has been deployed.
3. A complete list of all the references considered during the writing of this document is available at the end, in the "Reference" section.

2.2 Why Smart Skins

Observing the evolution of communication technologies since the end of the last century, a clear central idea emerges. Starting from the first generation of cellular networks, back when communications were analogic and portable devices were heavy and cumbersome, the direction of innovation has pushed the technology towards increasingly higher data-rates, which became a fundamental necessity with the introduction of smartphones and multimedia sharing, which are nowadays addressed by the faster and better focused data streams found in 4G and 5G implementations. The subsequent improvements considered for communication systems rely on the notion of multifunctionality, i.e., the property for a transmitting or receiving device to adapt to the working scenario and provide different services and functionalities accordingly, as a way to support more complex communication methods or services that rely on something more than the simple two-way communication between a base station and a user device. In recent years, researchers have therefore focused their attention on the study of possible ways to achieve this property in devices suitable for large scale consumer applications, and the literature is therefore rich of very hererogeneous proposals and ideas. A very promising approach is the one on which the present document is centered on, and relies on the concept of *smart skin*, a seemingly simple structure based on electromagnetic metamaterials able to offer a degree of performance and multifunctionality that makes it one of the most promising strategies for the communication market in the near future. A typical deployment of a similar structure would be the facade of a building in strategic points of a urban scenario, where it could be used to redirect the field coming from a nearby *base station* (BS) towards points where the signal would otherwise be lackluster, namely *blind spots*.

2.3 The State-of-the-Art

2.3.1 Physical fundamentals: Metamaterials, Metasurfaces and Metagratings

As mentioned, the underlying physical concept on which Smart skins are based is the wide and diverse field of electromagnetic metamaterials - which, from now on, will simply be referred to as metamaterials, albeit materials based on other physical properties exist. This kind of substances are artificial materials whose structure is engineered in a way that causes their overall behaviour to show properties that would otherwise be unobtainable with natural materials, generally thanks to a repeating structure of resonator-based unit cells. The research of metamaterials has grown impressively in the past decades, during which multiple applications have been found, many designs have been proposed and solutions have been hypothesized in order to tackle their inherent structural complexity, which is effectively one of the main downsides that characterize metamaterials. The main direction taken in this regard is very straightforward and consists in reducing the number of dimensions in which these materials are designed from three to two, obtaining a matrix of unit cells disposed on a plannar surface, resulting in what is fittingly called a metasurface. Even though these structures work with one less degree of freedom with respect to their parent technology, they offer properties and design possibilities similar to those of metamaterials, and therefore they have found employment in a wide variety of applications, which was facilitated also by their more simple manufacturing, which can generally be performed with traditional PCB techniques and machines. A particular typology of metasurface that is worth noting among the multitude of use cases is the phase-gradient metasurface, whose design is based on a gradual change in the structure's impedance, which in turn enables a rather flexible transformation of the wavefront of an impinging wave, resulting in changes to its overall direction, polarization and/o carried power. A slightly different approach to the same problem has emerged in the form of metagratings, a term that normally refers to a set of structures composed by an array of metamaterial-based scatterers distributed on a substrate in a more sparse manner with respect to metasurfaces, in a fashion that, as the name suggests, resembles a grate. This design choice allows a degree of control over the surface impedance consistently better than the one of metasurfaces, which are generally prone to poor efficiency and limited available steering angles, while maintaining a high level of freedom for choosing and redirecting the individual diffraction orders of the impinging signal. While the working principle of traditional metamaterials and metasurfaces is based on the notion that these devices can generally be considered as an homogeneous substance manifesting overall reversed optical phenomena, the functioning of metagratings is substantially different, as the sparseness of its elements prevents it to be treated as an homogeneous medium, and the desired properties have to be engineered considering the physical behaviour of each single unit cell. The research in this field, which in turn has seen an impressive acceleration in the last few years, indicates metagratings as a simple yet effective technology to achieve functionalities such as wave rerouting and manipulation.

2.3.2 Smart Skins

Many communication systems nowadays aim at achieving a high level of multifunctionality, i.e., obtaining a set of different functions for the system from a single antenna device, in order to improve the number of operations that the system itself can be used for, and therefore providing the users inside it a higher quality of service. In this perspective, research work has developed towards the employment of the properties of metamaterials in this field, where the concept of a

planar device capable of offering multifunctionality and good communication performance while maintaining excellent efficiency and a low level of weight and encumbrance has taken the name of smart skin. More specifically, the term *metamaterial smart skin* is most commonly used to refer to two different implementations:

- Metagrating-based smart skins, which are passive reflective metagratings able to select or discard singular diffraction orders of an impinging wave that can subsequently be employed for the realization of configurable passive antennas able to steer an impinging signal in almost any desired direction;
- Reconfigurable or Space-Time Modulated Metasurfaces, structures that combine the spatial discretization of metasurfaces with a time-coded periodic cycling of the reflection coefficient, which paves the way to the engineering of a set of different functionalities exploiting such a singular structure.

Both these implementation technologies (metagratings and space-time metasurfaces) are a really hot topic in the research on metamaterials, as they are rightfully considered a powerful tool to integrate in - or even use as a foundation of - future communication systems and cellular networks.

3 Metasurface Behaviour Analysis for Reflection Manipulation of EM Waves

3.1 Problem Statement

As mentioned in the introduction of this document, the goal of the activity is to achieve a convincing simulation of a smart EM environment centered on a smart skin based on the study on metasurfaces proposed by Danufane *et al.*, in order to pair it with an optimization tool and achieve a set of solutions for a possible deployment.

The focus of the analysis of this section will be on the reflective behaviour (i.e., the condition in which Tx and Rx are on the same hemisphere with respect to the metasurface) of the metasurface formulation proposed by Danufane *et al.*. Although the underlying concepts remain the same and the final formulations present relatively small differences, the transmission regime is not considered, as it does not fit with the final test case in which the device would be deployed. In fact, the final goal will be the employment of these metasurfaces as tiles on a smart skin deployment on the facade of a building inside a defined environment, in order to obtain a device embedded inside a wall able to redirect an impinging signal as needed, as represented in Figure 1.

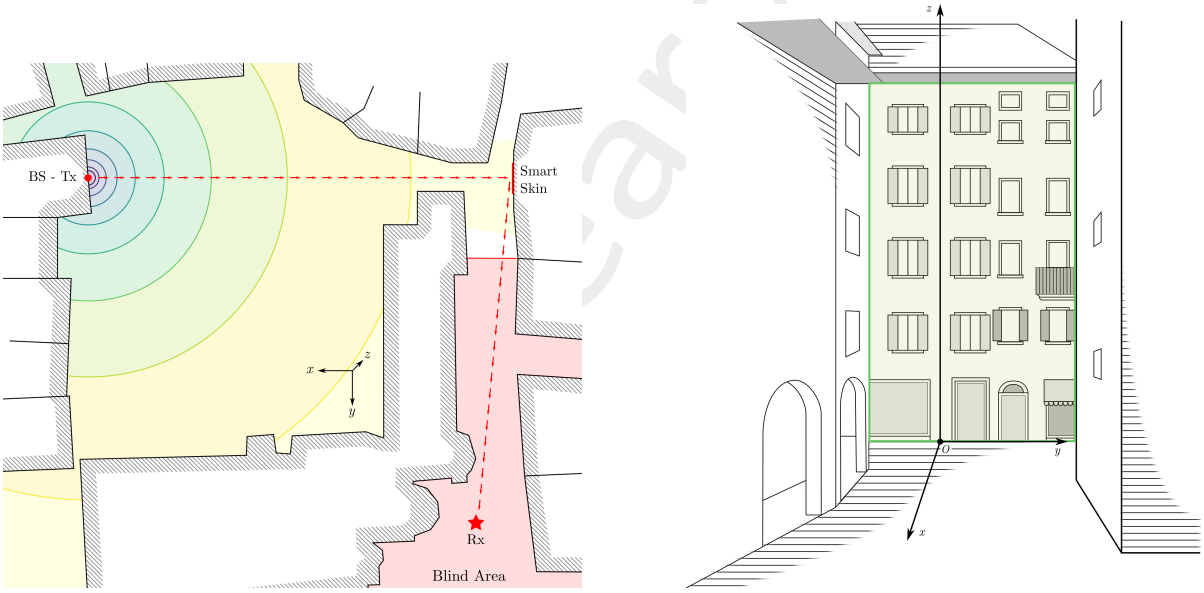

(*a*) Top-down representation of an expeced communication scenario

(*b*) A plausible site for the deployment of an EM smart skin

Figure 1: Conceptualization of a communication scenario for the deployment fo the EM smart skin as the final goal of the presented activity

3.1.1 F_R expression definition

This subsection will analyze the different formulations of the electric field contribution F_R provided by the metasurface $\mathcal{S}$ when the working regime is set to reflection.

For convenience, the relevant table rows are reported in the following Table I, where:

- The first column, "$\mathcal{S}$ **Configuration**", indicates the three different working configurations in which the metasurface can operate:

– *Specular reflection*, when the angle of the reflected wave is equal to the angle of the incident one, similar to Snell's reflection;

– *Anomalous reflection*, when the angle of the reflected is different to the incident one, and can be chosen by the designer;

– *Focusing*, when incident wave is reflected towards a focusing point, with the angle it would have if it had hit a traditional reflective lens.

- The second column, **"Approx."**, refers to the regime in which the surface is considered, so:

  – Electrically-large approximation denotes the electromagnetic behaviour of the surface $\mathcal{S}$ at a distance comparable to the surface dimensions, corresponding with the Fraunhofer definition of reactive near-field.

  – Electrically-small approximation denotes the electromagnetic behaviour of the surface $\mathcal{S}$ at a distance much larger than the surface dimensions, corresponding with the Fraunhofer definition of far-field. Generally speaking, this scenario allows to approximate oscillatory components in the integral expression of F_R into simpler and more easily readable defining relations.

  – Upper limit, for the focusing configuration, is used in place of the electrically-small approximation when it is not possible to enforce it, and it indicates the upper bound on the value of F_R when the physical dimensions of $\mathcal{S}$ tend to infinity.

- The last column, "$F_R(\mathbf{r}_{Rx})$ **expression**", reports the mathematical formulation of the term $F_R(\mathbf{r}_{Rx})$, which indicates the received field contributions caused by the reflection on the surface $\mathcal{S}$, for each considered subcase.

Table I: Defining equations for the reflection configuration of the metasurface $\mathcal{S}$.

$\mathcal{S}$ **Configuration**	**Approx.**	$F_R(\mathbf{r}_{Rx})$ **expression**
Specular Ref.	Elec. Large	$F_R(\mathbf{r}_{Rx}) \approx \frac{\lvert\Gamma_{ref}(x_\mathcal{S},y_\mathcal{S})\rvert\Omega_{ref}(x_\mathcal{S},y_\mathcal{S};\hat{\mathbf{p}}_{ref},\hat{\mathbf{p}}_{rec})}{4\pi(d_{Tx}(x_\mathcal{S},y_\mathcal{S})+d_{Rx}(x_\mathcal{S},y_\mathcal{S}))} e^{-jk(d_{Tx}(x_\mathcal{S},y_\mathcal{S})+d_{Rx}(x_\mathcal{S},y_\mathcal{S})-(\phi_0+\phi_{ref}+\phi_{rec})/k)}$
	Elec. Small	$F_R(\mathbf{r}_{Rx}) \approx \frac{jk\Gamma_{ref}\Omega_{ref}(0,0,\hat{\mathbf{p}}_{ref};\hat{\mathbf{p}}_{rec})L_xL_y(\cos\theta_{inc0}+\cos\theta_{rec0})}{4\pi d_{Tx0}d_{Rx0}} \mathrm{sinc}(kL_x\mathcal{D}_x)\mathrm{sinc}(kL_y\mathcal{D}_y)e^{-jk(d_{Tx0}+d_{Rx0}-(\phi_0+\phi_{ref}+\phi_{rec})/k)}$
Anomalous Ref.	Elec. Large	$F_R(\mathbf{r}_{Rx}) \approx \frac{\lvert\Gamma_{ref}(x_\mathcal{S},y_\mathcal{S})\rvert\Omega_{ref}(x_\mathcal{S},y_\mathcal{S};\hat{\mathbf{p}}_{ref},\hat{\mathbf{p}}_{rec})e^{-jk(d_{Tx}(x_\mathcal{S},y_\mathcal{S})+d_{Rx}(x_\mathcal{S},y_\mathcal{S})-(\alpha_{Rx}x_\mathcal{S}+\beta_{Ry}y_\mathcal{S})-(\phi_0+\phi_{ref}+\phi_{rec})/k)}}{8\pi\sqrt{\mathcal{R}_1(d_{Tx}(x_\mathcal{S},y_\mathcal{S}))^2+\mathcal{R}_2(d_{Rx}(x_\mathcal{S},y_\mathcal{S}))^2+\mathcal{R}_3 d_{Tx}(x_\mathcal{S},y_\mathcal{S})d_{Rx}(x_\mathcal{S},y_\mathcal{S})}}$
	Elec. Small	$F_R(\mathbf{r}_{Rx}) \approx \frac{jk\Gamma_{ref}\Omega_{ref}(0,0;\hat{\mathbf{p}}_{ref},\hat{\mathbf{p}}_{rec})L_xL_y(\cos\theta_{inc0}+\cos\theta_{rec0})}{4\pi d_{Tx0}d_{Rx0}} \mathrm{sinc}(kL_x\mathcal{D}_{\alpha R})\mathrm{sinc}(kL_y\mathcal{D}_{\beta R})e^{-jk(d_{Tx0}+d_{Rx0}-(\phi_0+\phi_{ref}+\phi_{rec})/k)}$
Focusing Ref.	Elec. Large	$F_R(\mathbf{r}_{Rx}) \approx \frac{jke^{j(\phi_0+\phi_{rec}+\phi_{ref})}}{16\pi^2} \iint \Omega_{ref}(x,y;\hat{\mathbf{p}}_{ref},\hat{\mathbf{p}}_{rec}) \frac{\lvert\Gamma_{ref}(x,y)\rvert(\cos\theta_{inc}(x,y)+\cos\theta_{rec}(x,y))}{d_{Tx}(x,y)d_{Rx}(x,y)}dxdy$
	Upper Lim.	$\lvert F_R(\mathbf{r}_{Rx})\rvert \leq C_{ref}\left(1+\frac{z_{P2}}{z_{P1}}\right)\tan^{-1}\left[\frac{(x_{P1}-x)(y_{P1}-y)}{z_{P1}\sqrt{(x_{P1}-x)^2+(y_{P1}-y)^2+z_{P1}^2}}\right]\Bigg\rvert_{x=-L_x;y=-L_y}^{x=L_x;y=L_y}$
	Elec. Small	$F_R(\mathbf{r}_{Rx}) \approx \frac{jk\Gamma_{ref}\Omega_{ref}(0,0;\hat{\mathbf{p}}_{ref},\hat{\mathbf{p}}_{rec})L_xL_y(\cos\theta_{inc0}+\cos\theta_{rec0})}{4\pi^2 d_{Tx0}d_{Rx0}} e^{j(\phi_0+\phi_{rec}+\phi_{ref})}$

The terms appearing in these expressions are hereby explained:

- $(x_{\mathcal{S}}, y_{\mathcal{S}})$ are the coordinates of a point on the surface $\mathcal{S}$, defined as a solution of the following system of equations:

$$\frac{(x_{\mathcal{S}} - x_{Tx})}{d_{Tx}(x_{\mathcal{S}}, y_{\mathcal{S}})} + \frac{(x_{\mathcal{S}} - x_{Rx})}{d_{Rx}(x_{\mathcal{S}}, y_{\mathcal{S}})} = 0, \qquad \frac{(y_{\mathcal{S}} - x_{Tx})}{d_{Tx}(x_{\mathcal{S}}, y_{\mathcal{S}})} + \frac{(y_{\mathcal{S}} - x_{Rx})}{d_{Rx}(x_{\mathcal{S}}, y_{\mathcal{S}})} = 0$$

  where $d_{\{Tx;Rx\}}(x_{\mathcal{S}}, y_{\mathcal{S}})$ is the distance of that point from the transmission and reception respectively;

- $\Gamma_{ref}(x_{\mathcal{S}}, y_{\mathcal{S}})$ is the metasurface reflection coefficient, a complex function engineered according to the desired behaviour of $\mathcal{S}$;

- $\Omega_{ref}(x_{\mathcal{S}}, y_{\mathcal{S}}; \hat{\mathbf{p}}_{ref}, \hat{\mathbf{p}}_{rec})$ is a term introduced to make the equation more readable, and takes the following form:

$$\Omega_{ref}(x_{\mathcal{S}}, y_{\mathcal{S}}; \hat{\mathbf{p}}_{ref}, \hat{\mathbf{p}}_{rec}) = \frac{k^2}{\epsilon_0} p_{dm} (\tilde{\mathbf{p}}_{rec} \cdot \tilde{\mathbf{p}}_{ref} - (\hat{\mathbf{s}}_{(x,y)} \cdot \tilde{\mathbf{p}}_{rec})(\hat{\mathbf{s}}_{(x,y)} \cdot \tilde{\mathbf{p}}_{ref})) \mathcal{E}(\hat{\mathbf{p}}_{inc}, \hat{\mathbf{p}}_{ref})$$

  where the vector terms $\hat{\mathbf{p}}_{\{inc,ref,rec\}}$ indicate the polarization vector, having amplitude $\tilde{\mathbf{p}}_{\{inc,ref,rec\}}$, for the incident wave, the reflected one and the one at Rx, p_{dm} is the modulus of the dipole moment (as the source is considered a dipole), k is the wavenumber, $\hat{\mathbf{s}}_{(x,y)}$ is a unit-norm vector from Tx to a generic point $\mathbf{s} \in \mathcal{S}$, and $\mathcal{E}(\hat{\mathbf{p}}_{inc}, \hat{\mathbf{p}}_{ref})$ is the efficiency of the polarization conversion from $\hat{\mathbf{p}}_{inc}$ to $\hat{\mathbf{p}}_{ref}$;

- ϕ_0 is a fixed phase with value $\in [0, 2\pi[$, ϕ_{ref} is the phase of the components of $\hat{\mathbf{p}}_{ref}$, the polarization of the reflected wave, and ϕ_{rec} is the phase of the components of $\hat{\mathbf{p}}_{rec}$, i.e., the receiver polarization;

- L_x, L_y are the physical dimensions of the metasurface along the x and y axes, as reported in Figure 2;

- $\theta_{inc0}, \varphi_{inc0}$ are the polar angles of the incident wave from Tx to the centre of $\mathcal{S}$ ($x = 0$ and $y = 0$), and $\theta_{rec0}, \varphi_{rec0}$ are the polar angles of the received wave at Rx from the centre of $\mathcal{S}$, as seen in Figure 2;

- $d_{\{Tx0;Rx0\}}$ is the distance of the point $(0, 0)$, the centre of $\mathcal{S}$, with Tx and Rx respectively (see again Figure 2);

- $\mathcal{D}_x$ and $\mathcal{D}_y$ are terms related to the integral approximation in the electrically small regime and they take the following form:

$$\begin{aligned} \mathcal{D}_x &= \sin\theta_{inc0}\cos\varphi_{inc0} + \sin\theta_{rec0}\cos\varphi_{rec0} \\ \mathcal{D}_y &= \sin\theta_{inc0}\sin\varphi_{inc0} + \sin\theta_{rec0}\sin\varphi_{rec0} \end{aligned}$$

- α_R and β_R are design parameters ($\in \mathbb{R}$) that allow the desired customization of the *anomalous reflection* configuration:

$$\begin{aligned} \alpha_R &= -\sin\theta_{inc0}\cos\varphi_{inc0} - \sin\theta_{rad}\cos\varphi_{rad} \\ \beta_R &= -\sin\theta_{inc0}\sin\varphi_{inc0} - \sin\theta_{rad}\sin\varphi_{rad} \end{aligned}$$

  where θ_{rad} and φ_{rad} are the polar angles of the desired direction of radiation;

- $\mathcal{R}_{\{1,2,3\}}$ are terms related to the integral approximation in the electrically-large regime, and are defined as:

$$\begin{aligned}\mathcal{R}_1 &= \cos^2\theta_{rec}/(\cos\theta_{inc}+\cos\theta_{rec})^2\\ \mathcal{R}_2 &= \cos^2\theta_{inc}/(\cos\theta_{inc}+\cos\theta_{rec})^2\\ \mathcal{R}_3 &= (\cos^2\theta_{inc}+\cos^2\theta_{rec}+\sin^2\theta_{inc}\sin^2\theta_{rec}\sin^2(\varphi_{inc}-\varphi_{rec}))/(\cos\theta_{inc}+\cos\theta_{rec})^2\end{aligned}$$

- $\mathcal{D}_{\alpha R}, \mathcal{D}_{\beta R}$ are the shorthand notations for the following expressions: $\mathcal{D}_{\alpha R} = \alpha_R + \mathcal{D}_x$, $\mathcal{D}_{\beta R} = \beta_R + \mathcal{D}_y$;
- C_{ref} is the shorthand notation for the following expression: $C_{ref} = \dfrac{2k^3 p_{dm}\Gamma_{ref}\mathcal{E}(\hat{\mathbf{p}}_{inc}, \hat{\mathbf{p}}_{ref})}{16\pi^2\epsilon_0}$;
- $(x_{\{P1,P2\}}, y_{\{P1,P2\}}, z_{\{P1,P2\}})$ are the cartesian coordinates of the points $P1$ and $P2$ defined as $(P1, P2) = (Tx, Rx)$ *or* $(P1, P2) = (Rx, Tx)$.

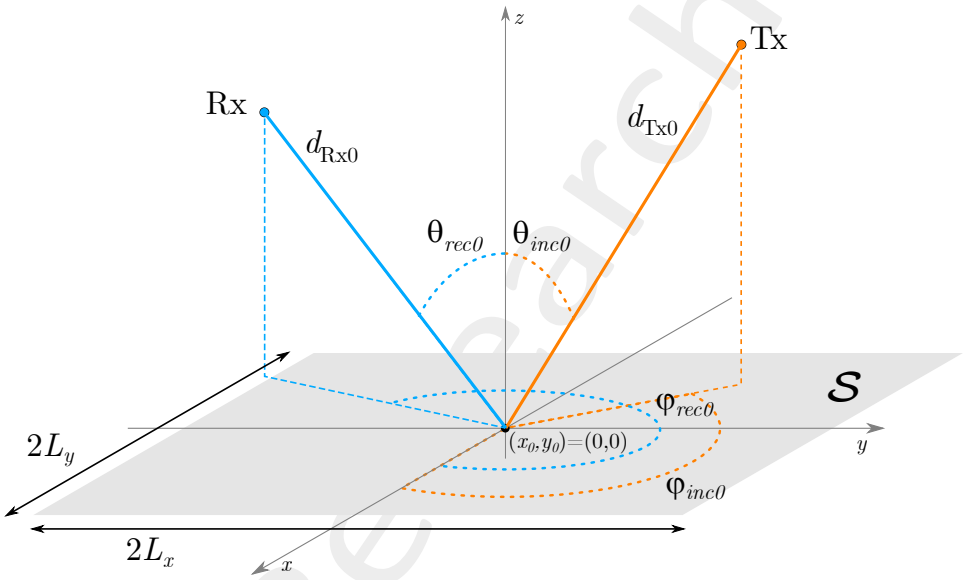

Figure 2: Resuming diagram with a graphic indication of the relevant parameters used for the definition of F_R

3.1.2 Effect of design parameters on F_R

After having reported the complete expressions that characterize the effect of the metasurface $\mathcal{S}$ on the received EM field, it is interesting to point out directly the design parameters that allow the device to behave in the desired way according to the above-mentioned formulas.

1. The metasurface physical dimensions, L_x and L_y appear directly in the formulation of the far field response of $\mathcal{S}$, implying a direct correlation between the size of $\mathcal{S}$ and the strength of the impact it has on the total received field;
2. The metasurface's EM properties (ϵ_r, μ_r) aren't considered directly as design parameters, but are instead confined to the formulation of the term Γ_{ref}, which is not addressed by the authors in , that becomes particularly interesting in the case of anomalous (i.e., non-specular) reflection;

3. The defining properties of the source and the receiver are considered through the factor Ω_{ref} and the polarization vectors $\hat{\mathbf{p}}_{\{inc,rec\}}$ (it has to be noted that the presence of the term p_{dm}, the modulus of the dipole moment, is due to the choice in to have a dipole antenna as a source);

4. The system's physical properties, such as the distances Tx-$\mathcal{S}$-Rx (d_{Tx}, d_{Rx}) and the polar angles of the incident/received wave ($\theta_{\{inc,rec\}}, \varphi_{\{inc,rec\}}$) appear directly in multiple terms and trigonometric functions of the formulation of F_R.

3.2 Forward Model Development and Benchmark Validation

The mathematical analysis of the behaviour of the metasurface $\mathcal{S}$ has been practically verified via a softwore implementation of the above mentioned formulas. This software has been written using a combination of Fortran instructions and bash executables, and its correct functioning was tested against the results presented in.

3.2.1 Code implementation

As mentioned, the mathematical formulas have been implemented using the Fortran programming language. The justification for this choice lies in the easy access and use of Fortran mathematical libraries, which would help handling the complex formulas reported in the previous Section, and the convenience that a Fortran implementation would bring in terms of integration with the code of the following steps of the activity and the alignment with the research center's standards of coding.

The first code iteration, used for the results considered in this Chapter, was a very straightforward transposition of the mathematical concepts in , and therefore the metasurface was considered horizontal, extending in the *x*-*y* plane, and the incoming/radiating wave coordinates were provided as polar triplets with respect to the centre of the metasurface (just as in Figure 2). The final electric field contribution F_R would result in a complex number, which would then be decomposed into absolute value and phase, where the former would be used in the polar plots for the result validation.

For the graphical representation of the results, both the polar heatmaps of the radiated electric field and all the linear plots of the following chapters were obtained through specifically developed Gnuplot scripts, once again conforming to the research center's standards.

3.2.2 Result validation

To verify the correct functioning of the code, a series of simulations has been performed, in order to validate the obtained results against the reference and verify that the obtained electric field component is coherent with the expected behaviour.

The first validation of the results has been conducted on the polar heatmap of the electric field contribution F_R, trying to achieve the same behaviour as for the anomalous reflection. To do so, the metasurface parameters have been set as reported in Table II:

Table II: Setup parameters for Danufane results validation

f	28 [GHz]
$\phi_0,\ \phi_{inc},\ \phi_{ref},\ \phi_{rec}$	0
$\mathcal{E}(\hat{\mathbf{p}}_{inc}, \hat{\mathbf{p}}_{ref})$	1
$\lvert\Gamma_{ref}(x,y)\rvert$	1
θ_{inc0}	45 [deg]
φ_{inc0}	60 [deg]
θ_{rec0}	30 [deg]
φ_{rec0}	180 [deg]

The obtained result is reported in Figure 3 side by side with the original heatmap, where it is clear how the anomalous reflection behaviour is maintained.

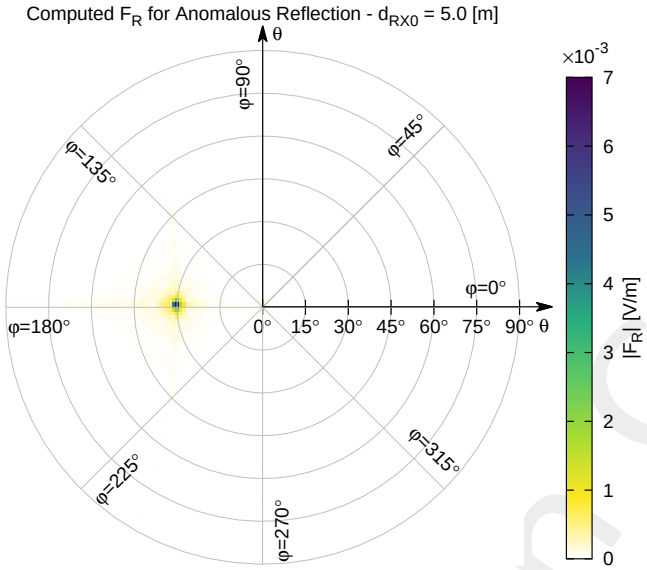

Obtained heatmap, $d_0 = 5$ [m]

Figure 3: Heatmaps for anomalous reflection regime of the metasurface $\mathcal{S}$

To further validate the obtained formula implementation, the results of both Specular and Anomalous reflection regimes are proposed in the following Figure 4, for two different TX/RX distances, where it emerges how both the regimes correctly achieve the expected results.

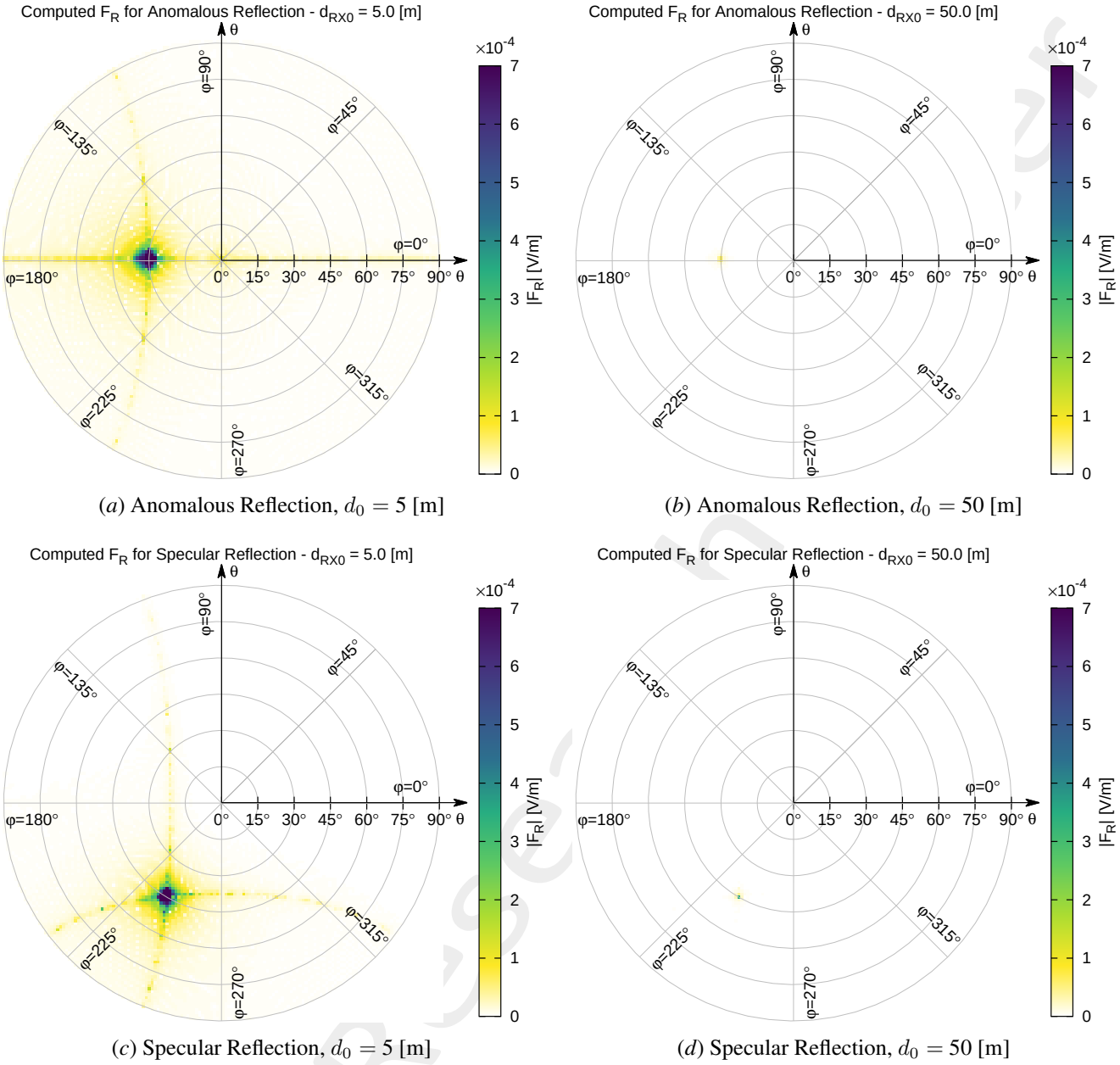

(*a*) Anomalous Reflection, $d_0 = 5$ [m]

(*b*) Anomalous Reflection, $d_0 = 50$ [m]

(*c*) Specular Reflection, $d_0 = 5$ [m]

(*d*) Specular Reflection, $d_0 = 50$ [m]

Figure 4: Heatmaps of the electric field F_R for the two working regimes of the metasurface $\mathcal{S}$

Subsequently, an additional validation of the obtained code has been provided by the replication of the graph by Danufane relating the distance of transmission and reception (both considered equal to a distance d_0) to the strength of the received electric field F_R. The results, reported in Figure 5, denote again a close similarity between the proposed code and the reference results, especially for what concerns the general trend of the curves and the effect that the size of $\mathcal{S}$ has on them.

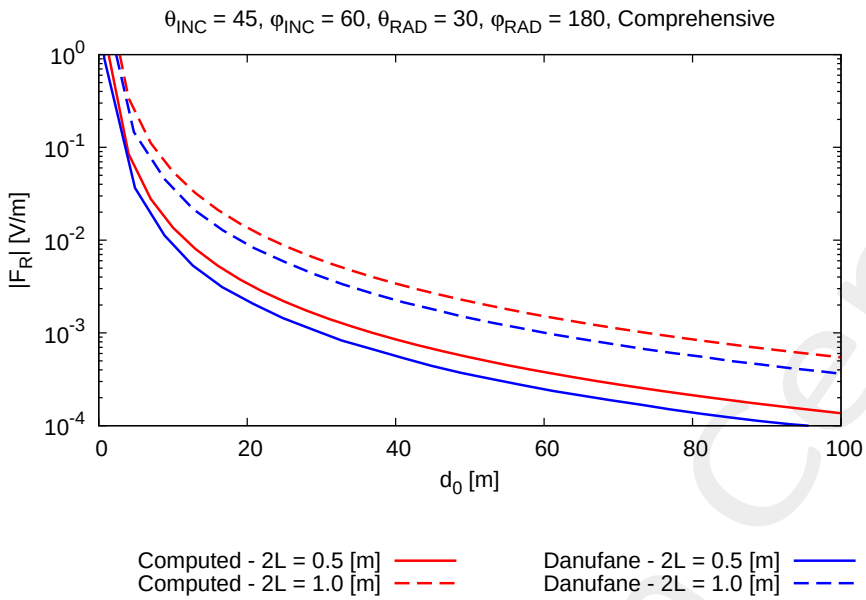

Figure 5: F_R field behaviour comparison between reference (*Danufane*, in blue) and obtained results (*Computed*, in red)

3.3 Parametric Analysis

After the behaviour of the software was proven in line with the results reported, additional simulations have been launched, each one with a varying parameter, to further investigate and represent on a visual level the behaviour of the metasurface $\mathcal{S}$, . The parameters that have been considered are hereby listed:

1. Metasurface side dimension, $2L_{\{x,y\}}$, as it is the most direct parameter that affects the strength of the field F_R reflected by the metasurface and one of the more easily controllable when designing the final device;
2. Incident wave elevation angle, θ_{inc0}, as a parameter on which it is relatively easy to act to obtain a stronger field for the receiver, and as a factor that could make a propagation path more efficient than others in a real-life scenario;
3. Distance of transmission and reception, $d_0 = d_{TX} = d_{RX}$, is indirectly considered in the parametric analysis as it was already studied as a mean for validating the results;
4. Metasurface asymmetry, that can be thought as the ratio $\frac{2L_x}{2L_y}$, was briefly considered for testing to understand the effects that non-ideal shapes of $\mathcal{S}$ - that are, once again, possible in a real-life application - could have on the final field F_R.

The results of these simulations will offer a deeper and more direct understanding of the influence the final design choices would have on the results; they are hereby reported in the following Subsections.

3.3.1 Effect of metasurface size - $2L_{\{x,y\}}$

A first test has been performed to study the behaviour of the metasurface $\mathcal{S}$ when its side dimension $2L_{\{x,y\}}$ was progressively increased. The results, reported in Figure 6, show, as expected, how the final field F_R increases for larger

metasurfaces and decreases for smaller ones. However, it is important to point out how this growth is not infinite, but stops when the dimensions of the surface $\mathcal{S}$ cause its non-compliance with the far-field hypotheses. This behaviour is mathematically justified by the presence of the terms L_x and L_y at the numerator in the expression of F_R.

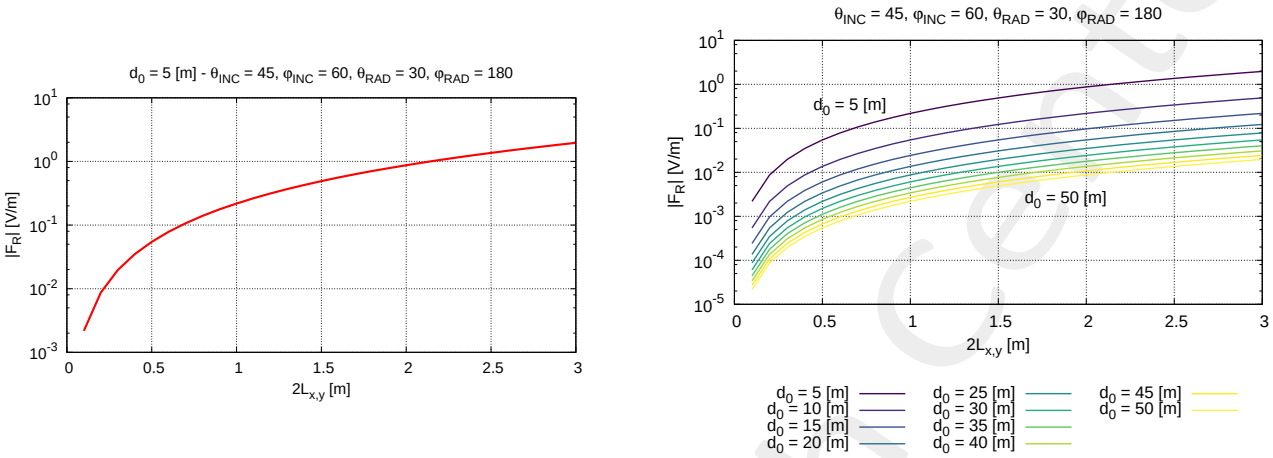

(*a*) F_R trend for $d_0 = 5$ [m]

(*b*) F_R trend for increasing values of d_0

Figure 6: F_R field behaviour when varying the metasurface size ($2L_{\{x,y\}}$)

If the field F_R is represented in a polar heatmap, it becomes even more clear how the choice of the size of the metasurface's side can impact the final communication scenario. In Figure 7 is noticeable how greater dimensions lead to larger and more powerful radiated beams; it is however important to notice how in a real life scenario larger sizes, such as $2L_{\{x,y\}} = 2.5$ [m] represented in Figure 7(*c*) should generally be avoided, as the Fraunhofer distance for which the antenna can be considered as being in far-field become larger than the distance of average users.

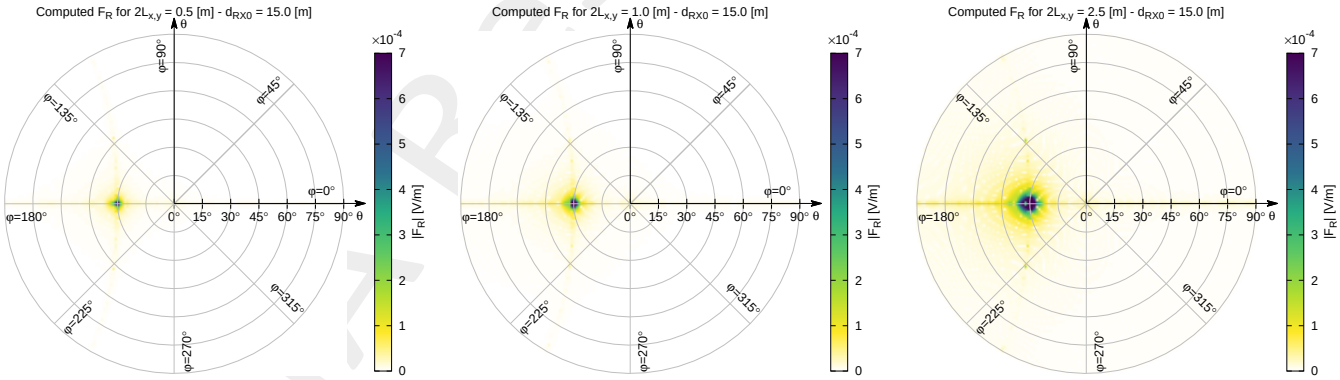

(*a*) $2L_{\{x,y\}} = 0.5$ [m]

(*b*) $2L_{\{x,y\}} = 1.0$ [m]

(*c*) $2L_{\{x,y\}} = 2.5$ [m]

Figure 7: Heatmaps of field F_R for different metasurface side sizes ($2L_{\{x,y\}}$)

3.3.2 Effect of incident angle - θ_{inc0}

A second test has been conducted to evaluate the behaviour of F_R when varying the elevation of the incident wave (i.e., the angle θ_{inc0}). As reported in Figure 8, for the considered polarization ($\hat{\mathbf{p}} = y$), illuminating the surface from an angle $\theta_{inc0} = 0$ [deg], i.e., directly from above, leads to a slightly stronger field at the receiver end. This behaviour can be logically explained considering how the effective illuminated area is the largest when illuminating the surface $\mathcal{S}$ from a

direction normal to it, and is mathematically justified in the formulas by the vector $\hat{\mathbf{s}}$ in the expression of Ω_{ref}.

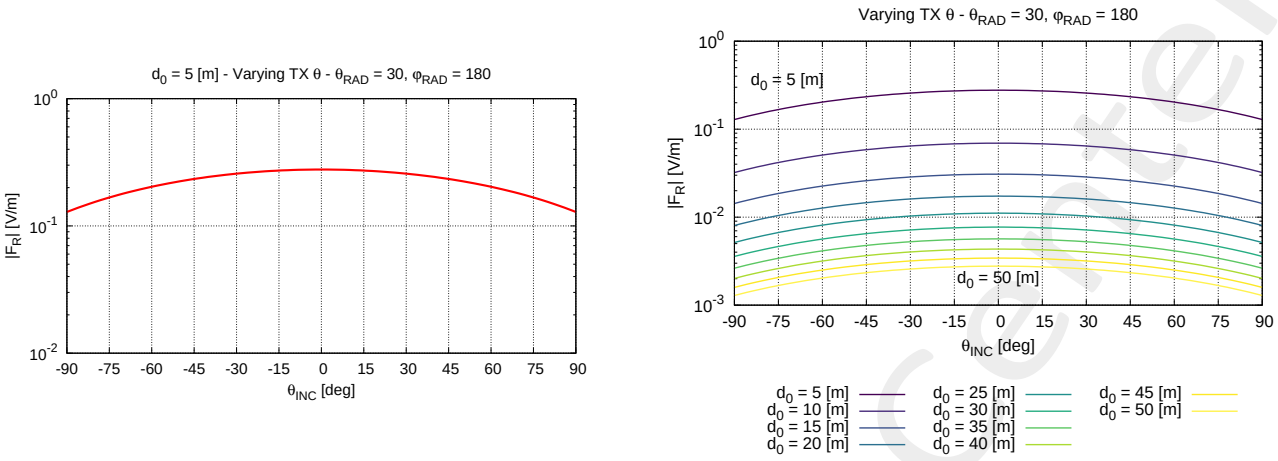

(*a*) F_R trend for $d_0 = 5$ [m]

(*b*) F_R trend for increasing values of d_0

Figure 8: F_R field behaviour when varying the incident wave elevation (θ_{inc0})

As in the previous case, the study of the heatmaps gives an immediate representation of the considered effect. In Figure 9 can be notice how the attenuation effect related to larger values of θ_{inc0} is present, albeit its negative impact on the overall field F_R is much smaller than the one related to the metasurface dimension. As a result, it can be deduced that for real-life applications the metasurface should be installed so that it is orthogonally illuminated by the transmitting antenna.

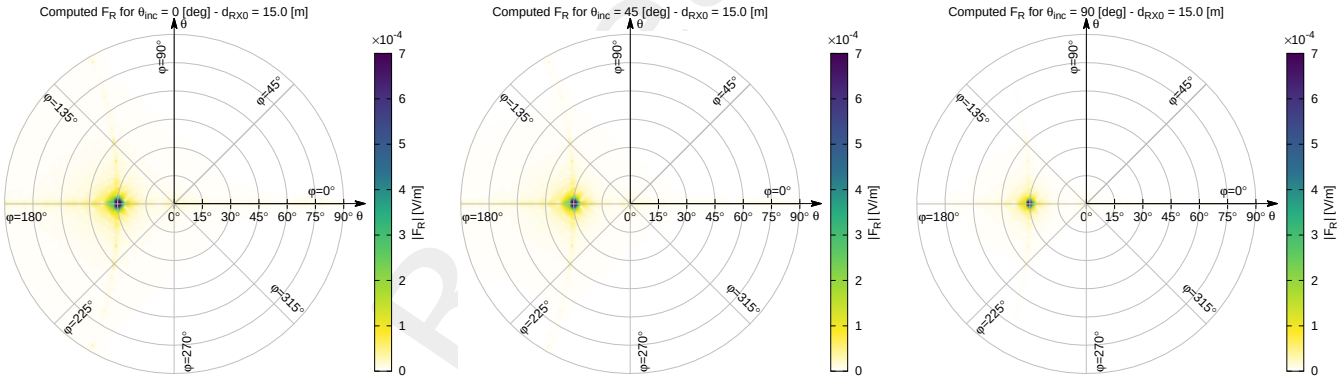

(*a*) $\theta_{inc0} = 0$ [deg]

(*b*) $\theta_{inc0} = 45$ [deg]

(*c*) $\theta_{inc0} = 90$ [deg]

Figure 9: Heatmaps of field F_R for different incident wave angles (θ_{inc0})

3.3.3 Additional notes

Effect of distance The effect of distance on the field F_R is indirectly considered throughout the parametric analysis [see Figures 6 (*b*) and 8 (*b*)] as it is the term that most influences the magnitude of the electric field F_R and that is generally not a design parameter that is freely modifiable in a real life scenario. Anyway, the effect of the transmission and reception distance is considered as a form of result validation in the dedicated section (Figure 5).

Metasurface asymmetry Some tests have been performed considering an asymmetric (non-square) metasurface, i.e., different values for $2L_x$ and $2L_y$. When their product is maintained equal (e.g. doubling one and halving the other), as expected from the formulas, the overall F_R remains equal, but some unwanted artifacts begin to appear, likely due to the

presence of the term $L_{\{x,y\}}$ in the *sinc* function that multiplies the field. As the presence of these artifacts can be noticed only for lower distances, when the surface does not fully respect the far-field hypotheses, this should not be a cause for concern, but strong asymmetry should be avoided as it drastically increases the maximum dimension of $\mathcal{S}$, which in turn leads to a more distant area in which the metasurface can operate in a far-field regime.

More information on the topics of this document can be found in the following list of references.

References

[1] Benoni, F. Capra, M. Salucci, and A. Massa, "Towards real-world indoor smart electromagnetic environments - A large-scale experimental demonstration," *IEEE Trans. Antennas Propag.*, vol. 71, no, 11, pp. 8450-8463, Nov. 2023 (DOI: 10.1109/TAP.2023.3305053).

[2] G. Oliveri, M. Salucci, and A. Massa, "Features and potentialities of static passive EM skins for NLOS specular wireless links," *IEEE Trans. Antennas Propag.*, vol. 71, no. 10, pp. 8048-8060, Oct. 2023 (DOI: 10.1109/TAP.2023.3301654).

[3] G. Oliveri, M. Salucci, and A. Massa, "Generalized analysis and unified design of EM skins," *IEEE Trans. Antennas Propag.*, vol. 71, no. 8, pp. 6579-6592, Aug. 2023 (DOI: 10.1109/TAP.2023.3281073).

[4] M. Salucci and A. Massa, "Unconventional sources for smart EM environments: An inverse scattering vision," *Reviews of Electromagnetics*, Invited Paper, vol 1, pp. 17-18, 2022 (DOI: 10.1109/MOCAST52088.2021.9493390).

[5] M. Salucci, A. Benoni, G. Oliveri, P. Rocca, B. Li, and A. Massa, "A multihop strategy for the planning of EM skins in a smart electromagnetic environment," *IEEE Trans. Antennas Propag.*, vol. 71, no. 3, pp. 2758-2767, Mar. 2023 (DOI: 10.1109/TAP.2022.3233714).

[6] G. Oliveri, F. Zardi, P. Rocca, M. Salucci, and A. Massa, "Constrained-design of passive static EM skins," *IEEE Trans. Antennas Propag.*, vol. 71, no. 2, pp. 1528-1538, Feb. 2023 (DOI: 10.1109/TAP.2022.3225593).

[7] G. Oliveri, P. Rocca, M. Salucci, D. Erricolo, and A. Massa, "Multi-scale single-bit RP-EMS synthesis for advanced propagation manipulation through system-by-design," *IEEE Trans. Antennas Propag.*, vol. 70, no. 10, pp. 8809-8824, Oct. 2022 (DOI: 10.1109/TAP.2022.3201700).

[8] A. Benoni, M. Salucci, G. Oliveri, P. Rocca, B. Li, and A. Massa, "Planning of EM skins for improved quality-of-service in urban areas," *IEEE Trans. Antennas Propag. - Special Issue on 'Smart Electromagnetic Environment'*, vol. 70, no. 10, pp. 8849-8862, Oct. 2022 (DOI: 10.1109/TAP.2022.3177284).

[9] G. Oliveri, F. Zardi, P. Rocca, M. Salucci, and A. Massa, "Building a smart EM environment - AI-Enhanced aperiodic micro-scale design of passive EM skins," *IEEE Trans. Antennas Propag. - Special Issue on 'Smart Electromagnetic Environment*,' vol. 70, no. 10, pp. 8757-8770, Oct. 2022 (DOI: 10.1109/TAP.2022.3151354).

[10] P. Rocca, P. Da RÙ, N. Anselmi, M. Salucci, G. Oliveri, D. Erricolo, and A. Massa, "On the design of modular reflecting EM skins for enhanced urban wireless coverage," *IEEE Trans. Antennas Propag. - Special Issue on 'Smart Electromagnetic Environment*,' vol. 70, no. 10, pp. 8771-8784, Oct. 2022 (DOI: 10.1109/TAP.2022.3146870).

[11] G. Oliveri, P. Rocca, M. Salucci, and A. Massa, "Holographic smart EM skins for advanced beam power shaping in next generation wireless environments," *IEEE J. Multiscale Multiphys. Comput. Tech.*, vol. 6, pp. 171-182, Oct. 2021 (DOI: 10.1109/JMMCT.2021.3121300).

[12] A. Massa, A. Benoni, P. Da RÙ, S. K. Goudos, B. Li, G. Oliveri, A. Polo, P. Rocca, and M. Salucci, "Designing smart electromagnetic environments for next-generation wireless communications," *Telecom*, Invited Paper, vol. 2, pp. 213-221, 2021 (DOI: 10.3390/telecom2020014).